Available online at www.sciencedirect.com

jmr&t Journal of Materials Research and Technology

www.jmrt.com.br

Original Article

Experimental and numerical studies on formability of extra-deep drawing steel in incremental sheet metal forming

*Suresh Kurra**, *Srinivasa Prakash Regalla*

Department of Mechanical Engineering, Birla Institute of Technology and Science Pilani, Hyderabad Campus, Hyderabad, India

ARTICLE INFO

Article history:
Received 20 January 2014
Accepted 17 March 2014
Available online 13 April 2014

Keywords:
Incremental forming
Formability
Maximum wall angle
Thickness distribution
Finite element simulation
EDD steel

ABSTRACT

This paper focuses on the formability and thickness distribution in incremental sheet forming (ISF) of extra-deep drawing steel (EDD). In ISF, the formability of the material is primarily measured by the maximum formable wall angle and maximum allowable thinning. The maximum wall angle is generally obtained by forming frustum of cones and square pyramids having different wall angles till fracture, which requires a large number of experiments. Therefore in the present study, a continuously varying wall angle conical frustum (VWACF) was used to predict the maximum wall angle to minimize the number of experiments. VWACF is generated using circular, parabolic, elliptical and exponential generatrices. In order to get the maximum allowable thinning, the thickness of the formed geometry has been measured at various points along the depth. In addition, the thickness distribution has been computed theoretically based on the sine law and also using finite element code LS-DYNA. Theoretical and simulated thickness values have been compared with measured thickness values. It was found from the results that the finite element model was more accurate than theoretical model in predicting thickness distribution.

1. Introduction

Incremental sheet forming (ISF) process has been identified as a potential and economically viable process for sheet metal prototypes and low volume production. The process is very flexible and can be carried out on a computer numerical control (CNC) milling machine, robots or specially designed machines for ISF applications. In this process, a flat sheet is held in a specially designed fixture and is deformed into required shape by a spherical-ended tool. The path of the tool is controlled by a part program generated using computer aided manufacturing (CAM) software. The main attractive features of this process are simple tooling and better forming characteristics than the conventional sheet metal forming processes. The process can be carried out without any die or with a partial die setup, made up of low cost material such as plastic or wood. The process has been demonstrated as a potential process for forming complex shapes, automotive service panels, head light casing and customized bio-medical

* *Corresponding author.*
E-mail: ksuresh.iitd@gmail.com (S. Kurra).
http://dx.doi.org/10.1016/j.jmrt.2014.03.009

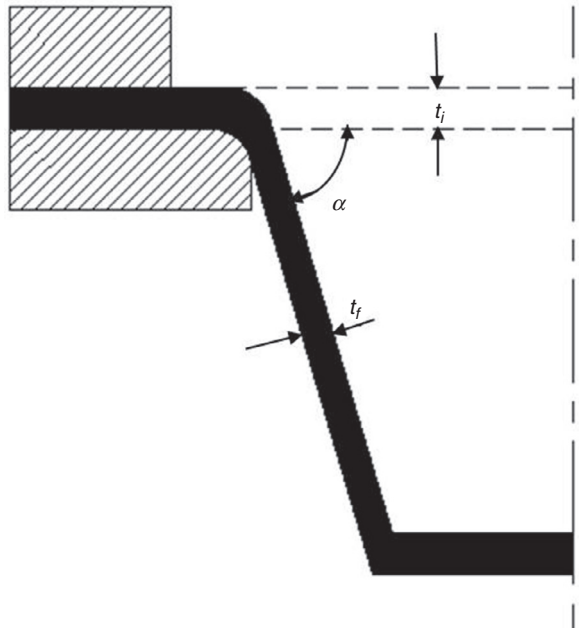

Fig. 1 – Schematic representation of thickness variation in incremental forming of constant wall angle parts.

parts such ankle support, plate prosthesis, implants for arthoplasty and cranial implants etc., [1,2].

In ISF, the sheet undergoes larger strains before its fracture, in comparison to common sheet metal operations such as deep drawing and stretching. Emmens et al. [3] proposed six different mechanisms to explain the increased formability in ISF, namely, contact stress; bending-under-tension; shear; cyclic straining; geometrical inability to grow and hydrostatic stress. These mechanisms delay the damage and increase the limit of fracture strain. Several studies [4–10] have been made to understand formability in ISF and various methods have been proposed for assessing the formability in ISF.

1.1. *Formability assessment by maximum wall angle*

In ISF, the wall thickness of the part varies as per sine law. If t_i and t_f are initial and final thickness of the part with wall angle α with horizontal plane, then the final thickness can be predicted by using the following relation [6]. The schematic representation of thickness variation in constant wall angle part is shown in Fig. 1.

$$t_f = t_i \cos\alpha \quad (1)$$

From Eq. (1), it is clear that with the increase in wall angle, the thickness tends to reach zero, which leads to fracture. Thus, the maximum wall angle and minimum allowable thickness to which the part can be formed without fracture can be used as the parameters for assessing the formability in ISF. Also, the maximum formable wall angle of the part varies linearly with thickness and is given by the following relation [6]:

$$\psi_{max} = kt_0 + \beta \quad (2)$$

where k is the slope of the line in deg/mm, t_o is the initial thickness of the blank and β is the y-intercept of the line.

Micari et al. [11] suggested a frustum of cone with top base diameter of 72 mm and height of 40 mm as a bench mark part to find the maximum wall angle. They have chosen this geometry because of lesser spring back during its forming. The benchmark specimen proposed by Micari et al. [11] provides a common basis for the determination of the maximum wall angle; however, it still requires a large amount of experimental work. To overcome this problem, Hussaini et al. [12] proposed different geometries with continuously varying wall angle along the depth of the part. These geometries are achieved by rotating the circular, parabolic, elliptic and exponential curve segments about an axis. In all these four parts the top base diameter was kept as 110 mm and the wall angle was varied from 40° to 80°.

Feed rate, rotational speed, step depth, tool diameter, lubrication, wall angle and toolpath are some of the most important parameters that affect the mechanics of ISF process. The process parameters also have significant effect on maximum wall angle. To study this, Ham and Jeswiet [13] used Box-Behnken Design of experiments and investigated the effect of various process parameters on maximum wall angle. Ambrogio et al. [14] analyzed the formability of light weight alloys in hot ISF by measuring the maximum formable wall angle. Palumbo and Brandizzi [15] studied the effect of static heating and tool rotational speed on formability in difficult-to-form materials such as Ti alloys. Ben Hmida et al. [16] studied the effect of grain size of the material on formability and forming forces in ISF of micro parts. Hussaini et al. [17] studied the effect of step depth, feed rate and diameter of the tool on maximum wall angle in cold ISF of titanium sheet.

Capece Minutolo et al. [18] formed the frustum of cone and pyramid with different slope angles from a sheet of 100 mm × 100 mm size. The cone had been formed with top base diameter 70 mm and depth 39 mm, and pyramid had been formed with top side length of 100 mm and maximum depth of 35 mm. They observed higher wall angles in conical parts compared to pyramidal parts. They also performed numerical simulations using LS-DYNA to analyze the formability. Bhattacharya et al. [19] studied the effect of tool diameter, step depth, sheet thickness and feed rate on the maximum wall angle. They formed the conical shape with different wall angles till the fracture. The study indicates that tool diameter, step depth and sheet thickness have significant effect on the maximum wall angle, while the effect of feed rate is negligible.

These studies indicate that there is no standard part geometry for finding maximum wall angle in ISF. To address this problem, EUREKA project was initiated in Europe and as a part of it, Tisza [20] formed the parts with constant and varying wall angles. He observed good agreement in the results between the constant and varying wall angle parts and showed the varying wall angle parts as a potential candidate for maximum wall angle prediction with minimum number of experiments.

The present work focuses on the investigation of ISF formability of extra-deep drawing (EDD) steel sheet, which is a widely used material in automotive applications involving simple and complex parts requiring high formability [21,22].

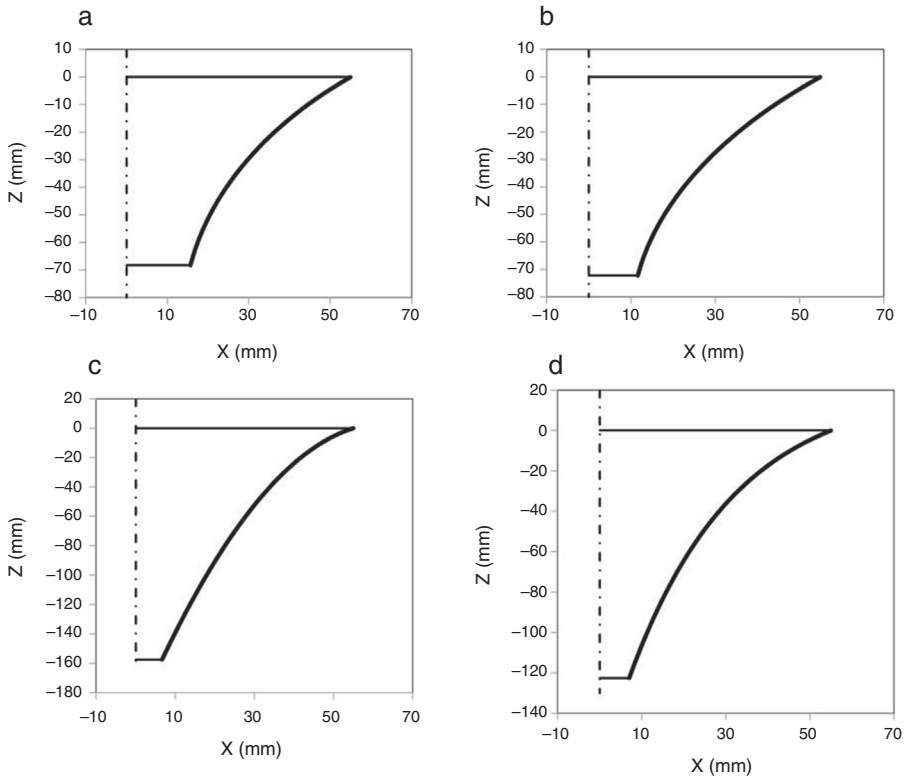

Fig. 2 – Different generatrices used for modeling the parts (a) circular generatrix (b) elliptical generatrix (c) parabolic generatrix (d) exponential generatrix.

Here, four varying wall angle conical frustums are used with circular, elliptical, parabolic and exponential generatrices as shown in Fig. 2. These curve segments are represented in parametric form due to their inherent advantages over explicit and implicit representation (Table 1). These parametric equations simplify mathematical formulations for predicting wall angle and thickness at any point p on the generatrix. In all the geometries, the top diameter is kept as 110 mm and the wall angle is varied from 40° to 80°. The variation of wall angle along the depth is shown in Fig. 3 for all four generatrices. In case of circular, elliptical and exponential generatrices, the wall angle variation is uniform along the depth, while in parabolic generatrix the wall angle is 73° for a depth of 50 mm and 7° for the remaining depth from 50 mm to 157.5 mm.

2. Experimental study

All the ISF experiments are performed on Bridgeport Hardinge 3-axis CNC milling machine with a fixture to hold the blank and a cylindrical tool with hemispherical head. The tool is made of EN36 and is heat treated to 60 HRC. The tool is polished with fine grade abrasive paper and lapping paste to improve the surface finish and to minimize the friction

Table 1 – Parametric equations of the curve segments used to design the parts (a) circular generatrix (b) elliptical generatrix (c) parabolic generatrix (d) exponential generatrix.

(a) $x(u) = 115\cos 2\pi(0.3611 + 0.1111u) + 128.94$ $z(u) = 115\sin 2\pi(0.3611 + 0.1111u) - 88.08$ $0 \le u \le 1$	(b) $x(u) = 160\cos 2\pi(0.3776 + 0.0968u) + 170$ $z(u) = 130\sin 2\pi(0.3776 + 0.0968u) - 90.38$ $0 \le u \le 1$
(c) $x(u) = 48.348u - 54.998$ $z(u) = -5(0.8402 + 4.8348u)^2 + 3.53$ $0 \le u \le 1$	(d) $x(u) = 48u - 55$ $z(u) = 4e^{0.04(41.5+48u)} - 21$ $0 \le u \le 1$

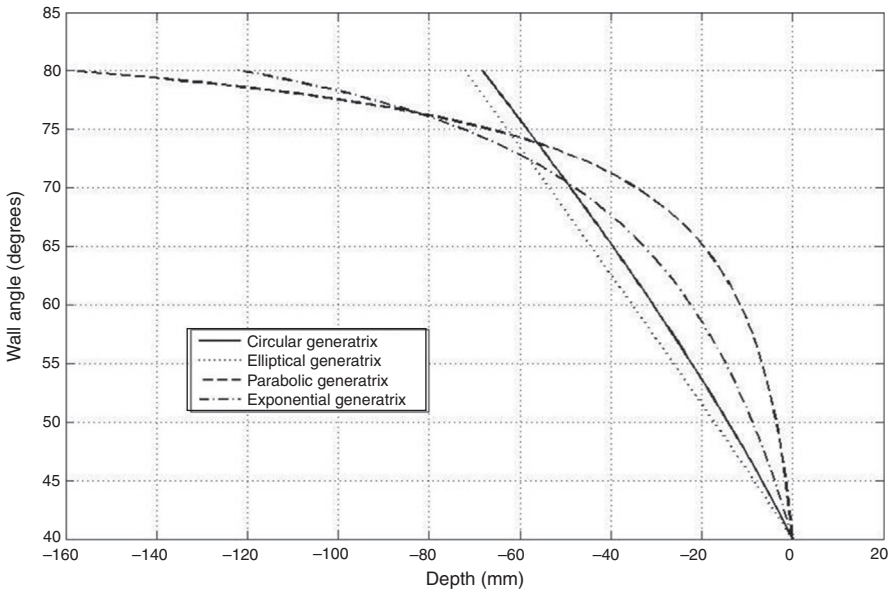

Fig. 3 – Variation of wall angle with depth for different geometries.

between the blank and sheet. A backing plate is provided below the blank to prevent the bending of the sheet and to improve the form accuracy of the part. The backing plate is of 250 mm × 250 mm × 12 mm in size with 110 mm diameter hole in the center. The edge of the circular hole is provided with 5 mm radius to prevent the tearing of sheet due to sharp corners. EDD steel sheet of 250 mm × 250 mm × 1 mm size is used as a blank material to make different parts. SAE-40 lubricating oil is applied to minimize the friction and temperature between the blank and tool. All the experiments are performed with 10 mm diameter tool at 750 mm/min feed rate and 0.5 mm step depth. The schematic diagram of the process and complete experimental setup are shown in Figs. 4 and 5 respectively.

To generate the tool path for the part geometries, the curve segments are designed in Pro-E software using the parametric equations given in Table 1. These curves are rotated about an axis to get the final part geometry with top base diameter of 110 mm. The parametric equations of resultant surfaces are given in Table 2. The generated tool paths for different geometries are shown in Fig. 6 and formed parts are shown in Fig. 7.

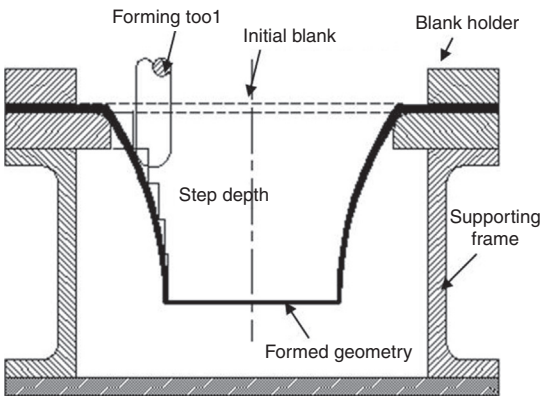

Fig. 4 – Schematic representation of ISF process.

Material properties for numerical simulations are obtained using uni-axial tensile test. ASTM E8 sub-size specimens are used to test the mechanical properties of EDD steel sheet. The experiments are performed with a cross-head velocity of 2 mm/min. The load-displacement data obtained from computer controlled universal testing machine have been used to calculate the engineering stress (S) and engineering strain (e) using relations (3) and (4). The stress–strain data have been used to get the true stress (σ) – true strain (ε) data using Eqs. (5) and (6) assuming constant specimen volume. The true stress–true strain curve of EDD steel sheet is shown in Fig. 8a. In sheet metal forming operation, the material generally undergoes the stresses beyond yield point and below the ultimate stress point. In this region the material undergoes the strain hardening and stress–strain curve in this region has been approximated by the power law Eq. (7) [23].

$$S = \frac{P}{A_0} \tag{3}$$

$$e = \frac{\Delta l}{L_0} \tag{4}$$

$$\sigma = S(1+e) \tag{5}$$

$$\varepsilon = \ln(1+e) \tag{6}$$

$$\sigma = K\varepsilon^n \tag{7}$$

Taking log on both sides the above equation becomes

$$\log\sigma = \log K + n\log\varepsilon \tag{8}$$

Fig. 5 – Experimental setup for incremental forming on CNC milling machine.

In the above equations A_0,L_0 and Δl represents the original cross-sectional area, gauge length and elongation of tensile test specimen respectively. Eq. (8) is an equation of straight line with x-axis as a log of true stress and y-axis as log of true strain (Fig. 8b). The slope of this line gives the strain hardening exponent (n) and y-intercept of the line gives the log of strength coefficient ($\log K$). Strain hardening exponent (n) measures how rapidly the material becomes harder and stronger. Higher the value of n, higher the formability. In addition to uni-axial tensile test, Ericson cupping test is performed to get the limiting dome height of the blank material. The mechanical properties and limiting dome height for EDD steel sheet from these tests are summarized in Table 3.

Table 2 – Parametric equations of the surfaces with (a) circular generatrix (b) elliptical generatrix (c) parabolic generatrix (d) exponential generatrix.

(a)
$x(u,v) = [115\cos 2\pi(0.3611 + 0.1111u) + 128.94]\cos 2\pi v$
$y(u,v) = [115\cos 2\pi(0.3611 + 0.1111u) + 128.94]\sin 2\pi v$
$z(u,v) = 115\sin 2\pi(0.3611 + 0.1111u) - 88.08$
$0 \le u \le 1$
$0 \le v \le 1$

(b)
$x(u,v) = [160\cos 2\pi(0.3776 + 0.0968u) + 170]\cos 2\pi v$
$y(u,v) = [160\cos 2\pi(0.3776 + 0.0968u) + 170]\sin 2\pi v$
$z(u,v) = 130\sin 2\pi(0.3776 + 0.0968u) - 90.38$
$0 \le u \le 1$
$0 \le v \le 1$

(c)
$x(u,v) = [48.348u - 54.998]\cos 2\pi v$
$y(u,v) = [48.348u - 54.998]\sin 2\pi v$
$z(u,v) = -5(0.8402 + 4.8348u)^2 + 3.53$
$0 \le u \le 1$
$0 \le v \le 1$

(d)
$x(u,v) = [48u - 55]\cos 2\pi v$
$y(u,v) = [48u - 55]\sin 2\pi v$
$z(u,v) = 4e^{0.04(41.5+48u)} - 21$
$0 \le u \le 1$
$0 \le v \le 1$

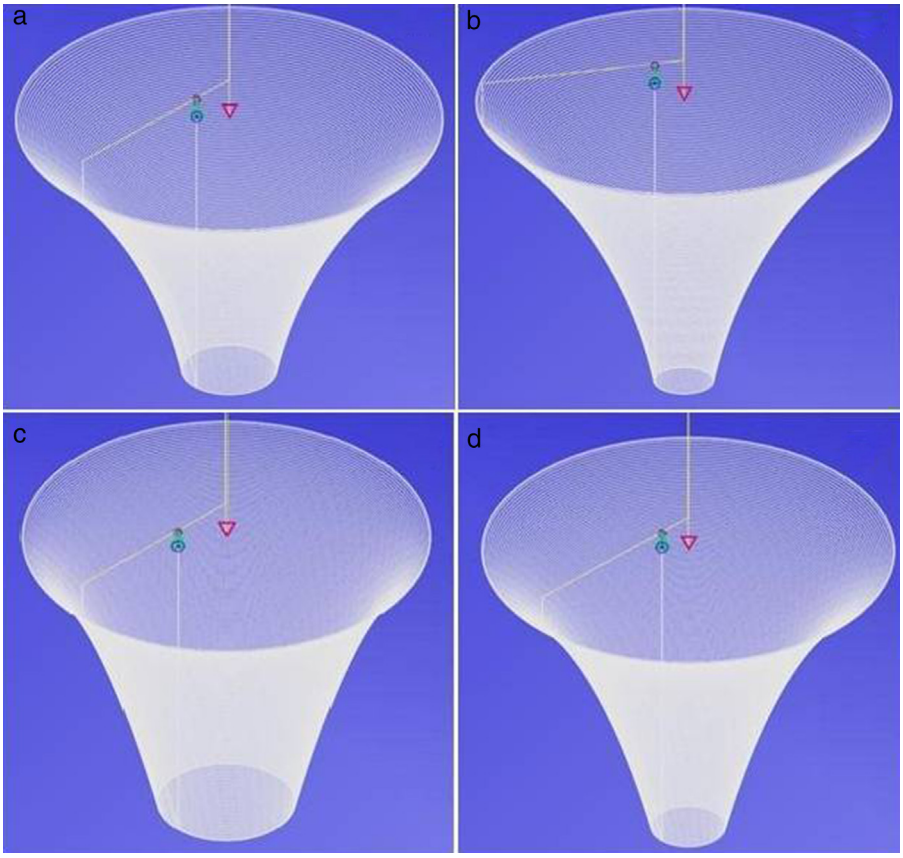

Fig. 6 – Generated tool paths for different geometries (a) circular generatrix (b) elliptical generatrix (c) parabolic generatrix (d) exponential generatrix.

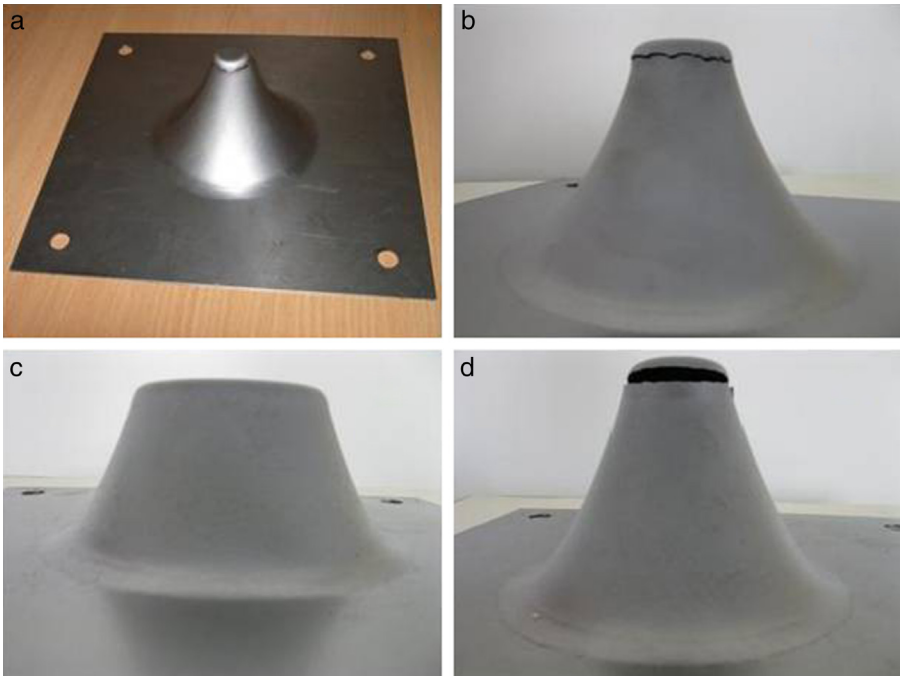

Fig. 7 – Parts formed in incremental forming (a) circular generatrix (b) elliptical generatrix (c) parabolic generatrix (d) exponential generatrix.

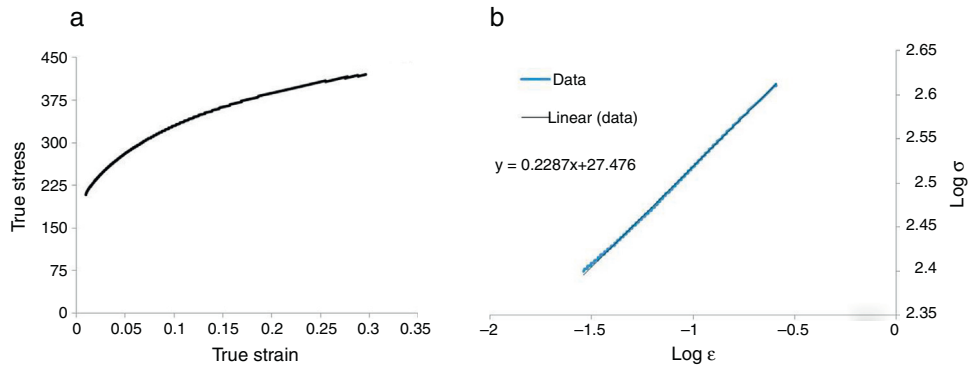

Fig. 8 – Mechanical properties of EDD steel sheet (a) true stress – true strain curve (b) log true stress vs. log true strain curve.

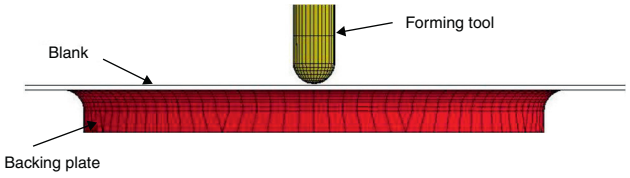

Fig. 9 – Finite element models of different tools in incremental forming.

3. Numerical simulation

A 3-D finite element model is developed in explicit finite element code LS-DYNA for numerical simulation of ISF process. The blank, die and forming tool are modeled with shell elements of type-2. Fine mesh is used for blank with element edge length of 1 mm. A total of five integration points are defined in thickness direction. The blank of EDD sheet is modeled using power law plasticity (MAT 18). The die and punch are modeled using the rigid material model (MAT 20). The strength coefficient and strain hardening exponent of blank are defined as 560 MPa and 0.23 respectively. The contact pairs, the tool and the blank, the blank and the die are modeled using forming one way surface to surface algorithm. Coulomb's friction law is used to model the friction between different contact surfaces. Due to the application of sufficient lubricating oil at tool sheet interface, very small friction efficient of 0.01 is used for simulations as recommended by Michael Elford et al. [24]. The finite element model of different tools is shown in Fig. 9.

Table 3 – Mechanical properties of EDD steel sheet.

Yield strength (in Mpa)	206
Ultimate strength (in Mpa)	337
% elongation	43
Strength coefficient (in Mpa)	560
Strain hardening exponent	0.23
Limiting dome height (in mm)	13.65

Unlike conventional processes, the toolpath for ISF is very complex and also 3-D in nature. Defining this complex toolpath in simulation software is a complex task. Most of the simulations in the past were performed using simplified toolpath rather than using the actual toolpath used for manufacturing the part [25]. In this paper, first the part is modeled using Pro-E software and the tool path is generated using manufacturing module in pro-E software. The toolpath is generated for all the four different geometries. The generated toolpath cannot be given as an input to the simulation software directly. Therefore, it is converted to time-position data using MATLAB routine, which is identical to the tool path used for manufacturing the part – this enhances the simulation model accuracy.

The length of toolpath in ISF is generally very long; as a result the computational time is very high. Mass scaling, and time scaling, adaptive meshing are some of the techniques proposed by various researchers to overcome this problem. In the present simulations, the punch velocity of 40 m/s and the mass scaling factor of 10 are used. A number of trial simulations are performed to select these parameters to see their influence on the computational time and on the dynamic effects. In all the simulations, the kinetic energy is found to be very less compared to the internal energy. This indicates that the selected process parameters are not inducing any dynamic effects in the model and the process is quasistatic in nature.

4. Results and discussion

The maximum wall angle is the primary parameter to assess the formability in ISF. To obtain the maximum wall angle, the varying wall angle conical frustums are formed on the CNC milling machine till the fracture. Two parts are formed for each generatrix design to improve the accuracy of results. After the occurrence of fracture the machine tool is stopped manually and the part is removed from the fixture. The depth of the part up to the fracture is measured using Vernier Height Gauge. The angle corresponding to this depth is called as the maximum formable angle, which is calculated using Eq. (9). The maximum wall angle is calculated for all eight parts and the

Table 4 – Thickness distribution in different part geometries along the depth.

Depth	Measured thickness	Theoretical thickness	Simulated thickness	% Error between measured vs. theoretical	% Error between measured vs. simulated
Part with circular generatrix					
0	1.000	0.765	1.000	23.41	0
2.5	0.980	0.744	0.964	24.06	1.63
5	0.845	0.722	0.803	14.50	4.97
7.5	0.740	0.700	0.700	5.40	5.40
10	0.711	0.679	0.661	4.50	7.03
15	0.654	0.635	0.617	2.82	5.65
20	0.608	0.592	0.573	2.63	5.75
25	0.571	0.548	0.528	3.94	7.53
30	0.518	0.505	0.483	2.50	6.75
35	0.483	0.461	0.438	4.43	9.31
40	0.429	0.418	0.389	2.54	9.32
45	0.368	0.374	0.333	1.79	9.51
50	0.323	0.331	0.309	2.50	4.33
55	0.308	0.287	0.284	6.59	7.79
60	0.272	0.244	0.250	10.22	8.08
62.5	0.236	0.222	0.253	5.76	7.20
Part with elliptical generatrix					
0	1.000	0.765	1.000	23.43	0
2.5	0.990	0.748	0.955	24.38	3.53
5	0.800	0.731	0.794	8.60	0.75
7.5	0.750	0.713	0.706	4.85	5.86
10	0.732	0.695	0.674	4.97	7.92
15	0.684	0.658	0.640	3.66	6.43
20	0.649	0.621	0.602	4.29	7.24
25	0.604	0.582	0.561	3.60	7.11
30	0.568	0.542	0.519	4.52	8.62
35	0.518	0.501	0.477	3.20	7.91
40	0.487	0.459	0.423	5.64	13.14
45	0.451	0.416	0.398	7.58	11.75
50	0.389	0.373	0.358	4.08	7.96
55	0.329	0.328	0.303	0.09	7.90
60	0.290	0.283	0.255	2.17	12.06
65	0.241	0.238	0.238	1.24	1.24
Part with parabolic generatrix					
0	1.000	0.765	1.000	23.44	0
2.5	0.970	0.673	0.963	30.58	0.72
5	0.880	0.607	0.777	30.92	11.70
7.5	0.678	0.558	0.589	17.62	13.12
10	0.587	0.519	0.494	11.49	15.84
15	0.480	0.461	0.421	3.95	12.29
20	0.434	0.418	0.387	3.54	10.82
25	0.386	0.386	0.350	0.05	9.32
30	0.357	0.360	0.321	0.89	10.08
35	0.336	0.338	0.300	0.86	10.71
40	0.330	0.321	0.283	2.72	14.24
45	0.289	0.305	0.267	5.74	7.61
50	0.290	0.292	0.258	0.79	11.03
53	0.241	0.286	0.255	18.75	5.80
Part with exponential generatrix					
0	1.000	0.765	1.000	23.43	0
2.5	0.973	0.728	0.955	25.11	1.84
5	0.818	0.693	0.786	15.26	3.91
7.5	0.724	0.659	0.665	8.92	8.14
10	0.684	0.627	0.607	8.21	11.25
15	0.600	0.570	0.546	4.93	9.00
20	0.533	0.520	0.496	2.32	6.94
25	0.482	0.477	0.451	0.93	6.43
30	0.448	0.440	0.41	1.74	8.48
35	0.414	0.407	0.375	1.52	9.42

Table 4 (*Continued*)

Depth	Measured thickness	Theoretical thickness	Simulated thickness	% Error between measured vs. theoretical	% Error between measured vs. simulated
40	0.386	0.379	0.346	1.76	10.36
45	0.362	0.354	0.315	2.15	12.98
50	0.326	0.332	0.297	1.87	8.89
55	0.311	0.312	0.281	0.48	9.64
60	0.291	0.294	0.292	1.34	0.34
65	0.286	0.279	0.291	2.41	1.74
70	0.271	0.264	0.275	2.25	1.47
75	0.242	0.252	0.252	4.13	4.13

Table 5 – Correlation coefficients for measured thickness vs. theoretical thickness and measured thickness vs. simulated thickness.

Part with	R^2 values	
	Measured vs. theoretical	Measured vs. simulated
Circular generatrix	0.9436	0.9944
Elliptical generatrix	0.9345	0.9933
Parabolic generatrix	0.9693	0.9827
Exponential generatrix	0.9659	0.9900

Table 6 – Descriptive statistics of error percentage in thickness distribution prediction.

	% of error statistics							
	Std. dev.		Mean		Max.		Min.	
	Theoretical	Simulated	Theoretical	Simulated	Theoretical	Simulated	Theoretical	Simulated
Circular generatrix	7.42	2.73	7.48	6.32	24.06	9.51	1.79	0
Elliptical generatrix	7.05	3.88	6.64	6.84	24.38	13.14	0.09	0
Parabolic generatrix	11.33	4.63	10.81	9.52	30.92	15.84	0.05	0
Exponential generatrix	7.59	4.04	6.04	6.39	25.11	12.98	0.48	0

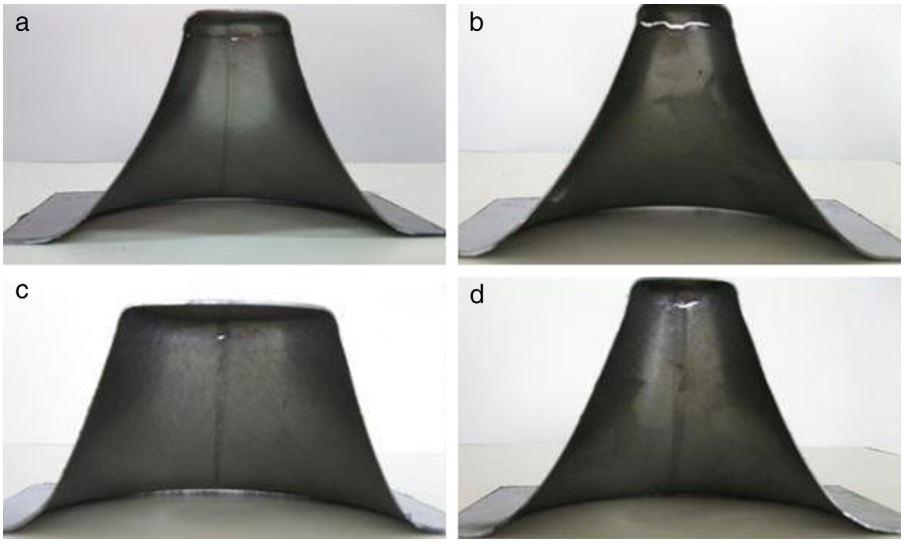

Fig. 10 – Cut sections of parts for thickness measurement (a) circular generatrix, (b) elliptical generatrix, (c) parabolic generatrix, (d) exponential generatrix.

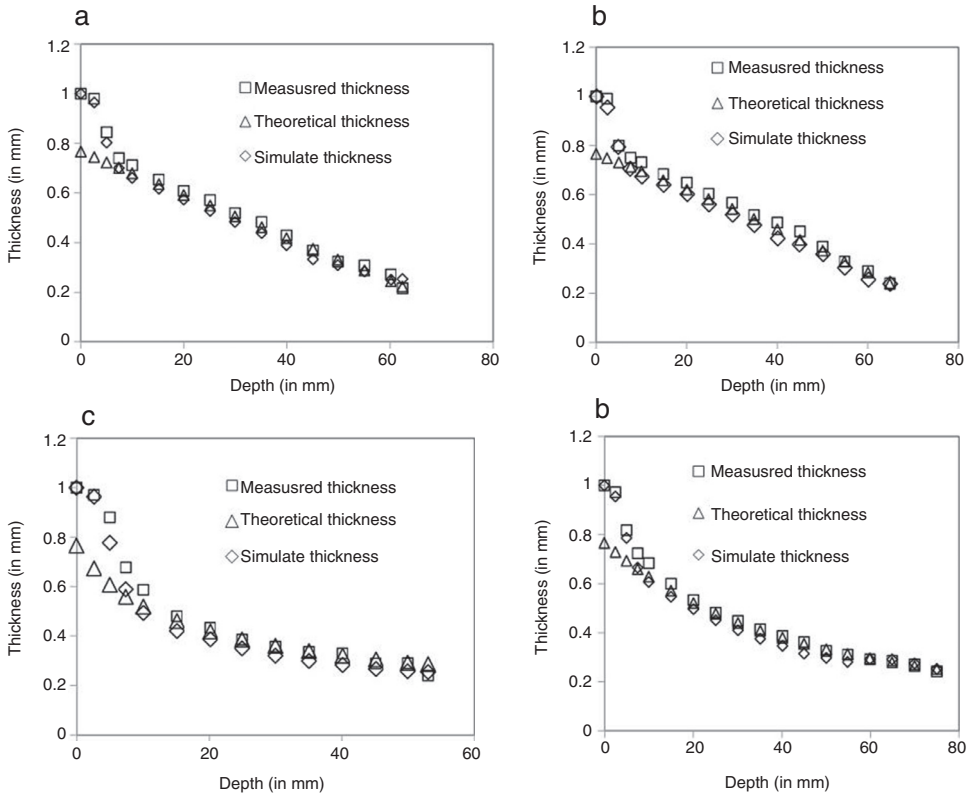

Fig. 11 – Distribution of thickness with depth (a) circular generatrix (b) elliptical generatrix (c) parabolic generatrix (d) exponential generatrix.

average value is taken as a liming wall angle for EDD steel in ISF.

$$\theta_p = \tan^{-1}\left(\frac{dz/du}{dx/du}\right) \tag{9}$$

In the above equation $(dz/du)/(dx/du)$ gives the slope at any point p on the generatrix with co-ordinates $x(u)$ and $z(u)$ and θp represents wall angle at p.

In order to get the thickness distribution along the depth, the parts are sectioned from the middle for ease of thickness measurement, and the cut parts are shown in Fig. 10. For measuring the thickness, the points are marked for every 5 mm from the top to the bottom of the part using Vernier Height Gauge. For better clarity of thickness distribution in the bending region, the points are marked for every 2.5 mm. Thickness at every point is measured using Digital Pointed Anvil Micrometer having a least count of 0.01 mm. In case of VWACF the wall angle and hence the thickness changes continuously with the depth. Hence, the wall angle (θ_p) and theoretical thickness (t_p) corresponding to each marked point (p) are calculated using Eqs. (9) and (10) respectively. Measured, theoretical and simulated thickness distribution for different geometries is shown in Table 4 and Fig. 11. Fig. 11 shows that the

Table 7 – Maximum wall angle and thinning limit with different geometries.

Part description	Part number	Depth at fracture (mm)	Wall angle (°)	Maximum thinning (mm)
Circular generatrix	1	62.5	77.15	0.236
	2	63.5	77.66	
Elliptical generatrix	1	62.0	74.60	0.241
	2	65.0	76.23	
Parabolic generatrix	1	50.0	73.00	0.290
	2	53.0	73.43	
Exponential generatrix	1	70.5	74.71	0.242
	2	75.0	75.40	

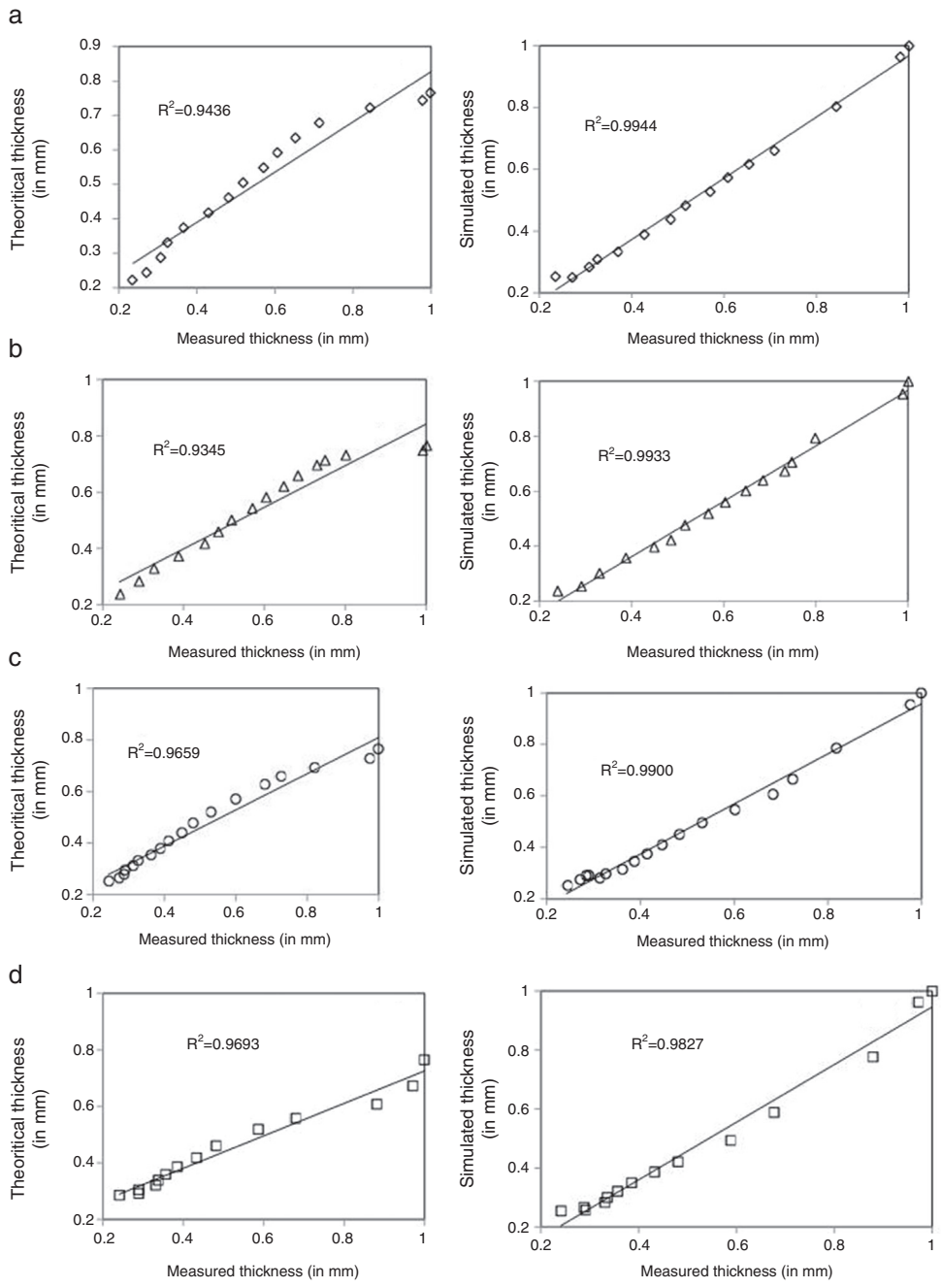

Fig. 12 – Correlation between measured vs. simulated and measured vs. theoretical thickness distribution in parts with (a) circular generatrix (b) elliptical generatrix (c) parabolic generatrix (d) exponential generatrix.

analytical model is poor in predicting thickness in the bending region, whereas numerical simulations are good in both bending and stretching regions. From Fig. 12, it is clear that a very good correlation was observed between measured and simulation results, when compared to the correlation between measured and analytical thickness distribution for all the geometries. The correlation coefficients and the error metrics for different part geometries are given in Tables 5 and 6 respectively. Based on the statistical parameters, it can be concluded that the simulation model is more accurate than analytical model in thickness prediction. Contour plots of thickness distribution from numerical simulations are shown in Fig. 13.

$$t_p = t_i \cos\theta_p \tag{10}$$

Depth, wall angle and maximum allowable thinning corresponding to the fracture point of various parts formed in ISF are summarized in Table 7. The values of maximum wall angles obtained with different geometries are close to each

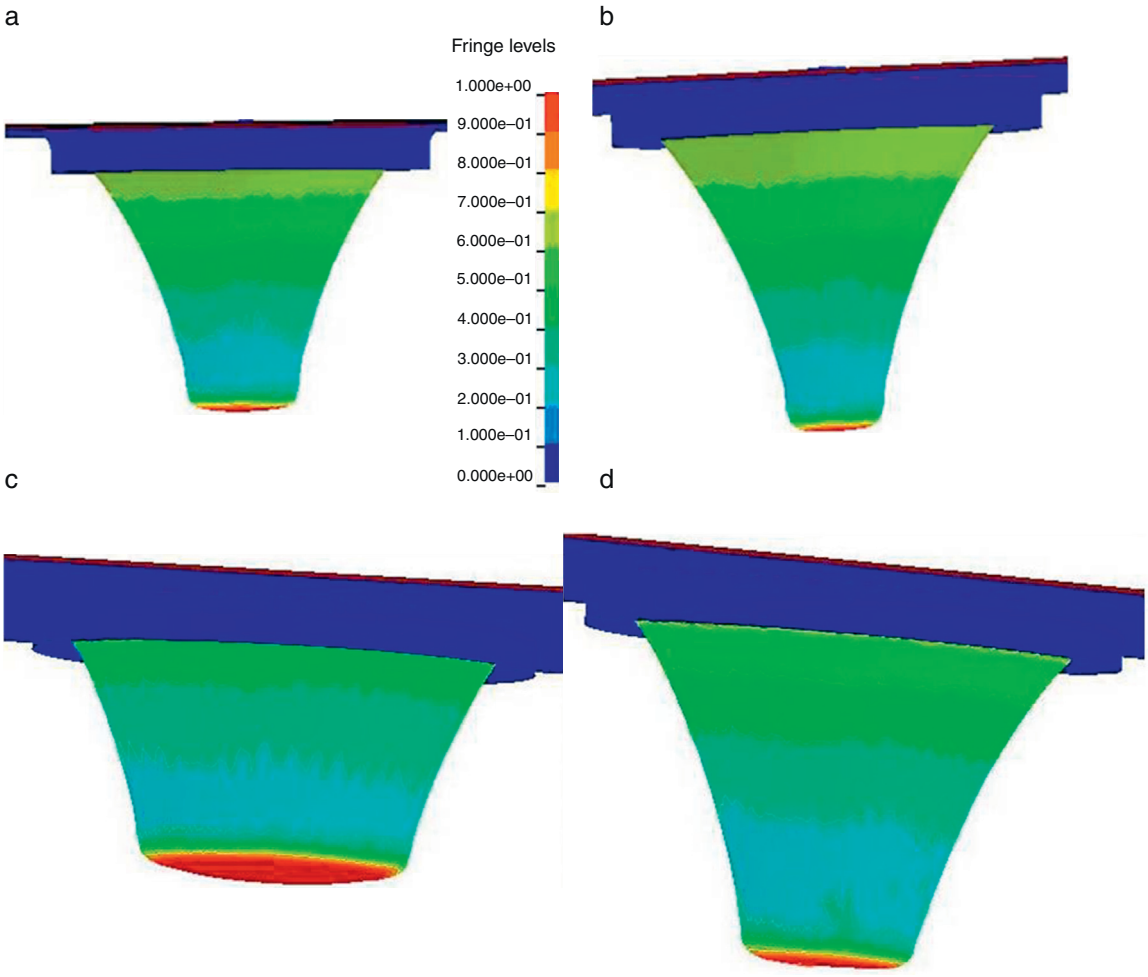

Fig. 13 – Contour plots of thickness distribution in parts with (a) circular generatrix (b) elliptical generatrix (c) parabolic generatrix (d) exponential generatrix.

other. The average value of maximum formable wall angle with EDD steel is computed as 75.27°. The maximum allowable thinning is 0.252 mm. The maximum variation in wall angle with different geometries is 4.6°. Lesser wall angle was obtained in part with parabolic generatrix; this could be due to steep variation in wall angle with this particular geometry. The variation in wall angle with different part geometries could be due to variation in slope distribution and curvature. Hussaini et al. [26] reported that the thickness of the sheet deviates from the sine law thickness at some point along its depth. They called this point as transition point and used it to measure the maximum allowable thinning. But, in this work, there is no such major deviation from the sine law thickness; therefore, the minimum thinning in the part is considered as the allowable thinning. Parts with circular, elliptical and exponential generatrices are good choices to consider as benchmark parts for maximum wall angle prediction in ISF. In case of parabolic generatrix, the variation in wall angle is very less after reaching certain depth. The wall angle computed using parts with varying wall angle conical frustums is generally more than the parts with constant wall angle. This is due to the larger force in case of constant wall angle parts compared to varying wall angle parts [12].

The fracture surface of the incrementally formed part is analyzed using SEM photographs. The fractured specimen is cut to the required size for fractography study. The low magnification fractured surface is shown in Fig. 14(a). The scanning electron microscope (SEM) photographs of fractured surface at higher magnifications are shown in Fig. 14(b–d); it indicates that the fracture is predominantly ductile in nature. In ductile fracture, damage accumulates due to nucleation, growth and coalescence of voids. Continuous nucleation of small voids takes place at the second phase particles and non-metallic inclusions (Fig. 14c) over a wide range of plastic strains. Continuous nucleation of small voids at second phase particles leads to material failure. It is clearly evident from Energy-dispersive X-ray spectroscopy (EDS) analysis (Fig. 15) that this inclusion could be aluminum oxide. The composition of inclusion from EDS study is presented in Fig. 15. The cleavage cracks could be due to inhomogeneous plastic deformation in fracture zone or the aluminum oxide inclusions. From SEM studies it can be concluded that the ductile fracture models such as

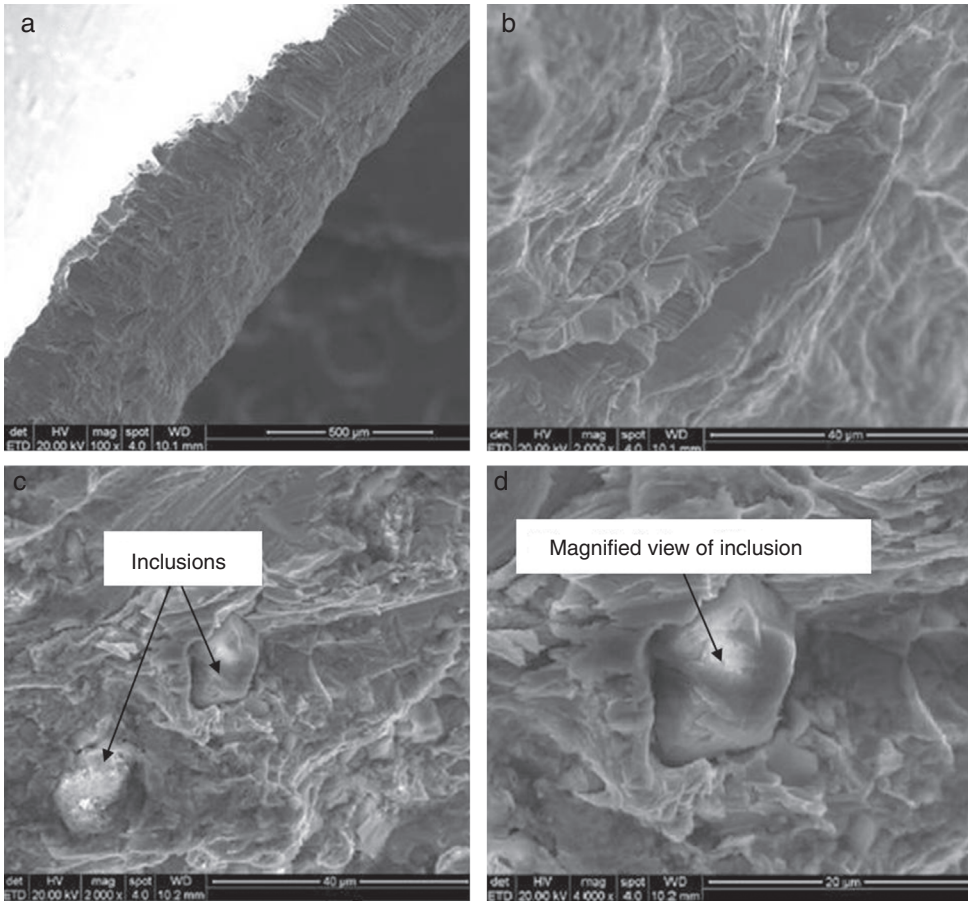

Fig. 14 – SEM photographs of fractured surface (a) fractured surface at low magnification, (b–d) at high magnification.

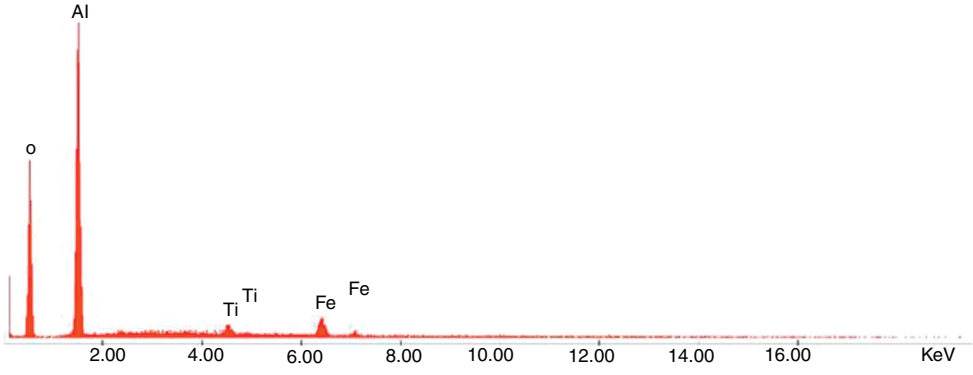

Fig. 15 – EDS analysis of inclusion.

Gurson, J-C and Lamatire can be used to model the fracture and for constructing the fracture forming limit diagram in ISF.

5. Conclusions

In this work, the maximum wall angle and the thinning limit of EDD steel sheet in single pass single point negative incremental forming have been investigated. For this purpose, parts with varying wall angle along the depth were formed till the fracture. Numerical simulations are performed following the experimental phase to get the thickness distribution using LS-DYNA. Thickness distribution obtained from numerical simulations was found to be more accurate than the values obtained from theoretical model. Theoretical model was found to be poor in predicting thickness in bending region, whereas the finite element model is good in predicting thickness in both the bending and stretching regions. A correlation coefficient of above 0.99 was observed between measured and simulated thickness with different part geometries. Limiting wall angle and allowable thinning were found to be 75.27° and 0.252 mm respectively. Maximum variation in wall angle with different generatrix curves was found to be 4.6°. This variation could be due to variation in the curvature and slope

distribution of different parts. Future study includes the construction of the fracture forming limit diagram (FFLD) for EDD steel sheets and the numerical simulations using finite element codes to study the distribution of strains and formability.

Conflicts of interest

The authors declare no conflicts of interest.

REFERENCES

[1] Jeswiet J, Micari F, Hirt G, Bramley A, Duflou J, Allwood J. Asymmetric single point incremental forming of sheet metal. CIRP Ann Manuf Technol 2005;54:88–114.

[2] Luisa Garcia-Romeu M, Pérez-Santiago R, Bagudanch I. Fabrication of a biopsy meso-forceps prototype with incremental sheet forming variants. Int J Mechtron Manuf Syst 2013;6:242–53.

[3] Emmens WC, Van den Boogaard AH. An overview of stabilizing deformation mechanisms in incremental sheet forming. J Mater Process Technol 2009;209:3688–95.

[4] Kim YH, Park JJ. Effect of process parameters on formability in incremental forming of sheet metal. J Mater Process Technol 2002;130:42–6.

[5] Filice L, Fratini L, Micari F. Analysis of material formability in incremental forming. CIRP Ann Manuf Technol 2002;51:199–202.

[6] Young D, Jeswiet J. Forming limit diagrams for single point incremental forming of aluminum sheet. IMECHE B J Eng Manuf 2005;219:1–6.

[7] Fratini L, Ambrogio G, Di Lorenzo R, Filice L, Micari F. Influence of mechanical properties of the sheet material on formability in single point incremental forming. CIRP Ann Manuf Technol 2004;53:207–10.

[8] Silva MB, Nielsen PS, Bay N, Martins PAF. Failure mechanisms in single-point incremental forming of metals. Int J Adv Manuf Technol 2011;56:893–903.

[9] Miklos T, Kovács PZ, Lukács Z. Preliminary studies on the determination of FLD for single point incremental sheet metal forming. Key Eng Mater 2012;504:863–8.

[10] Nguyen DT, Park JG, Lee HJ, Kim YS. Finite element method study of incremental sheet forming and its improvement for complex shape. IMECHE B J Eng Manuf 2010;224:913–24.

[11] Micari F, Ambrogio G. A common shape for conducting incremental forming tests. In: 1st Incremental Forming Workshop. University of Saarbrucken; 2004.

[12] Hussain G, Gao L, Dar NU. An experimental study on some formability evaluation methods in negative incremental forming. J Mater Process Technol 2007;186:45–53.

[13] Ham M, Jeswiet J. Forming limit curves in single point incremental forming. CIRP Ann Manuf Technol 2007;56:277–80.

[14] Ambrogio G, Filice L, Gagliardi F. Formability of lightweight alloys by hot incremental sheet forming. Mater Des 2012;34:501–8.

[15] Palumbo G, Brandizzi M. Experimental investigations on the single point incremental forming of a titanium alloy component combining static heating with high tool rotation speed. Mater Des 2012;40:43–51.

[16] Ben Hmida R, Thibaud S, Gilbin A, Richard F. Influence of the initial grain size in single point incremental forming process for thin sheets metal and microparts: experimental investigations. Mater Des 2013;45:155–65.

[17] Hussain G, Gao L, Zhang ZY. Formability evaluation of a pure titanium sheet in the cold incremental forming process. Int J Adv Manuf Technol 2008;37:920–6.

[18] Capece Minutolo F, Durante M, Formisano A, Langella A. Evaluation of the maximum slope angle of simple geometries carried out by incremental forming process. J Mater Process Technol 2007;194:145–50.

[19] Bhattacharya A, Maneesh K, Venkata Reddy N, Cao J. Formability and surface finish studies in single point incremental forming. Trans ASME J Manuf Sci Eng 2011;133:1020–8.

[20] Tisza M. General overview of sheet incremental forming. Manuf Eng 2012;55:113–20.

[21] Singh SK, Mahesh K, Gupta AK, Swathi M. Understanding formability of extra-deep drawing steel at elevated temperature using finite element simulation. Mater Des 2010;31:4478–84.

[22] Singh SK, Mahesh K, Gupta AK. Prediction of mechanical properties of extra deep drawn steel in blue brittle region using Artificial Neural Network. Mater Design 2010;31:2288–95.

[23] Dieter GE. Mechanical metallurgy. 3rd ed. New York: McGraw Hill Co.; 1986.

[24] Elford M, Saha P, Seong D, Ziaul Haque MD, Yoon JW. Benchmark 3 – incremental sheet forming. AIP Conf Proc 2013;1567:227–61.

[25] Chen LJ, Pei G, Fang Q, Pan J. A general method of numerical simulation for incremental forming. Adv Mater Res 2012;403–408:4084–8.

[26] Hussain G, Gao L. A novel method to test the thinning limits of sheet metals in negative incremental forming. Int J Mach Tools Manuf 2007;47:419–35.